An Electron Plasma Experiment to Study Vortex Dynamics Subject to Externally Imposed Flows

N. C. Hurst[1,a)], J. R. Danielson[1] and C. M. Surko[1]

[1] *University of California San Diego, 9500 Gilman Drive, La Jolla, CA 92093-0319*

[a)] nhurst@ucsd.edu

Abstract. An experimental technique is presented for studying two-dimensional (2D) ideal fluid vortices in the presence of externally imposed flows, using an electron plasma confined in a Penning-Malmberg trap. This procedure is made possible by an isomorphism between the Drift-Poisson equations governing electron plasma dynamics and the 2D Euler equations describing an ideal fluid. Here, the electron density is the analog of fluid vorticity, and the electric potential that of the fluid stream function. External flows are imposed in 2D using a segmented electrode spanning the length of the plasma. Details of the experimental procedure and data analysis are given, including the capabilities and limitations of the experimental approach.

INTRODUCTION

Two-dimensional (2D) ideal fluids have been studied in the laboratory using strongly magnetized pure electron plasma in a Penning-Malmberg trap as a model system [1]. In order to accomplish this, the plasma is prepared so that, in a particular range of temporal and spatial scales, the plasma dynamics perpendicular to the magnetic field are given by the Drift-Poisson equations

$$\left[\partial_t - \frac{1}{B}(\nabla_\perp \phi \times \hat{\mathbf{z}}) \cdot \nabla_\perp\right] \langle n \rangle_z = 0; \;\; \nabla_\perp^2 \phi = e\langle n \rangle_z / \varepsilon_0, \tag{1}$$

(in SI units) where ε_0 is the permittivity of free space, e is the electron charge, $\nabla_\perp = \partial_x \hat{\mathbf{x}} + \partial_y \hat{\mathbf{y}}$ is the gradient operator perpendicular to the magnetic field $\mathbf{B} = B\hat{\mathbf{z}}$ (assumed to be uniform throughout the domain), $\langle n \rangle_z$ is the z-averaged electron density, and the drift velocity is $\mathbf{v} = -\nabla_\perp \phi \times \hat{\mathbf{z}}/B$. These equations describe self-advection of the electron density due to the $\mathbf{E} \times \mathbf{B}$ drift. In a similar manner, the dynamics of a 2D ideal fluid can be described by self-advection of the vorticity field, as given by the 2D Euler equations

$$[\partial_t - (\nabla \psi \times \hat{\mathbf{z}}) \cdot \nabla] \omega = 0; \;\; \nabla^2 \psi = \omega, \tag{2}$$

where ψ is the fluid stream function in 2D, with fluid velocity $\mathbf{v} = -\nabla \psi \times \hat{\mathbf{z}}$ and vorticity $\omega = \nabla \times \mathbf{v}$. The Drift-Poisson equations (Eq. 1) and the 2D Euler equations (Eq. 2) are isomorphic under the substitutions $\phi/B \to \psi$ and $e\langle n \rangle_z / B\varepsilon_0 \to \omega$. Thus, the dynamics of the electron distribution $n(x, y)$ correspond directly to that of the vorticity distribution $\omega(x, y)$, and the electric potential ϕ is analogous to the stream function ψ.

Quasi-2D fluids are found in both natural and man-made environments. Examples include geophysical fluids (i.e., the oceans and atmospheres of Earth and other planets) [2], strongly magnetized laboratory plasmas ranging from confined antimatter plasmas [3] to toroidal fusion devices [4], astrophysical disks [5], airplane wakes [6], and mixing processes [7]. Although the dynamics of many of these systems are enriched by various non-2D or non-ideal effects, the Euler equations (Eq. 2) are a commonly used simple paradigm [8]. Inviscid conditions are difficult to create in the laboratory using traditional fluids (i.e., water tanks) [9], so the electron plasma presents a unique tool for studying 2D ideal fluid behavior.

Non-Neutral Plasma Physics X
AIP Conf. Proc. 1928, 020007-1–020007-10; https://doi.org/10.1063/1.5021572
Published by AIP Publishing. 978-0-7354-1620-8/$30.00

Prior results involving this plasma/fluid correspondence include the formation [10] and stability [11] of vortex crystals, vortex merger studies [12], turbulent cascade behavior [13], and inviscid damping of vortex distortions [14], to name a few. Most of these studies focused on the free relaxation of an initial vorticity distribution. However, when the boundary conditions of the cylindrical confining electrodes are specified, an externally imposed, irrotational $\mathbf{E} \times \mathbf{B}$ flow can be created, which advects the vorticity. Certain aspects of electron fluid dynamics under externally imposed electric fields have been investigated in Refs. [15] and [16].

In this paper, we describe an apparatus called the 8-Segment Trap (8ST) and the experimental procedures that we have recently developed to study ideal 2D fluid dynamics in the presence of externally imposed flows. A key feature of the apparatus is that the boundary conditions can be varied without violating the assumptions of the plasma/fluid analogy. It consists of a specially designed Penning-Malmberg trap for electron plasma where the boundary is divided into eight equal azimuthal segments that extend axially over the entire length of the plasma. A report of the first results from this device can be found in Ref. [17]. This paper consists of a discussion of the experimental apparatus and procedure, data analysis and calibration procedures, a discussion of the validity of the plasma/fluid analogy, examples of the type of results that can be obtained, and a set of concluding remarks.

EXPERIMENTAL APPARATUS

Figure 1 shows a schematic diagram of the 8ST apparatus. Shown are the electron source (A), cryopump (B), electrode structure (C), superconducting coils (D), and diagnostic equipment (E, F, G). The coils produce an axial magnetic field $B = 4.8$ T which is approximately uniform over the electrodes ($\delta B/B \sim 0.01$). The cryopump maintains a pressure of about 10^{-9} torr inside the chamber. The electron source is a heated tungsten cathode located in the flaring field region where $B_z \approx 0.03$ T. It produces electron beams of width ~ 5 mm and current ~ 1 μA. Electrodes I, III, and V are used for axial confinement; they are typically biased to $V_c = -100$ V. Electrode II is divided azimuthally into eight equal segments which can be independently biased; this is the region in which the fluid experiments take place. Electrode IV is divided azimuthally into four equal segments; these electrodes are used to control the plasma density profile *via* the Rotating Wall (RW) technique [3].

The diagnostic system consists of a phosphor screen (E) biased to +5 kV which is imaged through a window in the vacuum chamber and a lens (F) by a CCD camera (G). The phosphor screen is located in the flaring field region opposite the electron source, where $B_z \approx 1.2$ T. The wall radius of the 8ST is $r_w = 13$ mm, the length of the entire electrode structure is 440 mm, and the length of electrode II is 260 mm. Typical plasma parameters are total electron number $N = 10^8 - 10^9$, central electron density $n = 10^{13} - 10^{15}$ m^{-3}, temperature $T \approx 0.1$ eV, and plasma radius $r_p = 1 - 5$ mm.

EXTERNAL FLOW CAPABILITIES

During a fluid experiment the segments of electrode II are biased, creating vacuum electric fields which give rise to an irrotational $\mathbf{E} \times \mathbf{B}$ flow that advects the trapped electrons (i.e., the vorticity). In 2D, the electric potential inside the trap volume satisfies the Laplace equation $\nabla^2 \phi = 0$ with

$$\phi(r,\theta) = \sum_{m=0}^{\infty} \Big[A_m \cos(m\theta) + B_m \sin(m\theta) \Big] \Big(\frac{r}{r_w} \Big)^m, \tag{3}$$

where the A_m and B_m are expansion coefficients, given by

$$A_m = \frac{1}{\pi} \int \mathrm{d}\theta \cos(m\theta) \phi(r_w,\theta); \;\; B_m = \frac{1}{\pi} \int \mathrm{d}\theta \sin(m\theta) \phi(r_w,\theta), \tag{4}$$

where $\phi(r_w,\theta)$ is the applied boundary condition. Plasmas are typically prepared at the origin with $r_p \ll r_w$, so the lowest-order expansion terms are dominant. With the segmented electrodes aligned with the coordinate axes (x,y), the boundary conditions can often be chosen such that all $B_m = 0$.

Different choices of boundary conditions are shown in Fig. 2, including equipotential contours which are analogous to fluid streamlines. An external flow with a dominant $m = 1$ term can be created by biasing

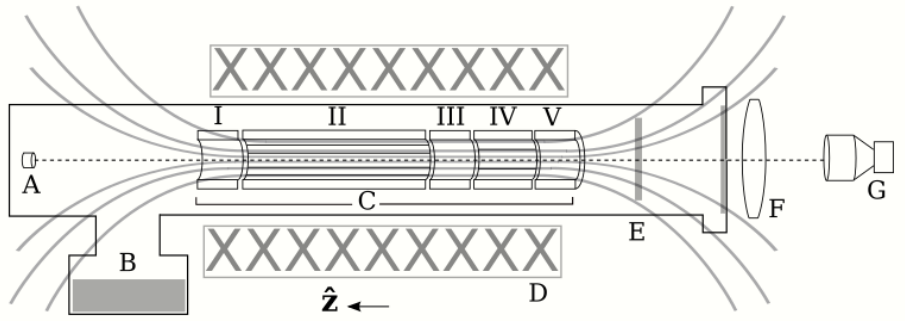

FIGURE 1. Schematic diagram of 8ST apparatus in the (y, z) plane, including electron source (A), cryopump (B), 8ST electrodes (C), magnet coils (D), phosphor screen (E), optical lens (F), and CCD camera (G). Magnetic field lines are shown schematically, as is a vacuum chamber enclosing the electrodes.

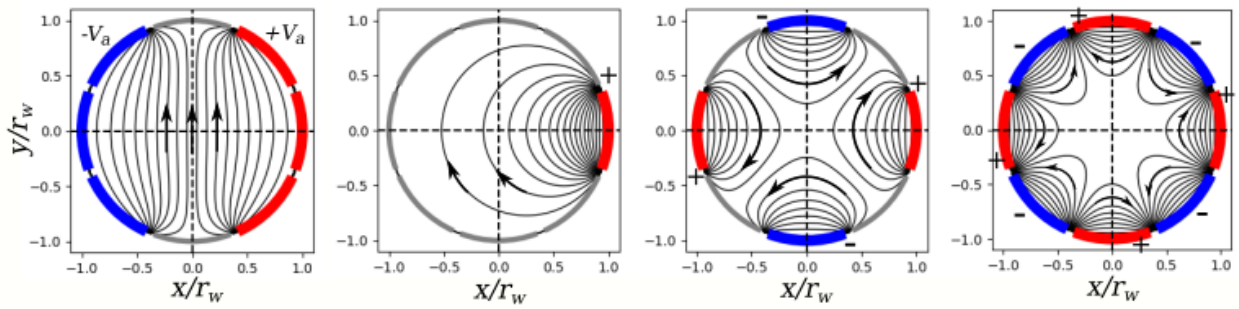

FIGURE 2. Choices of boundary conditions for electrode II, and the corresponding external flow field; (a) uniform vertical flow, (b) irrotational shear flow, (c) simple strain flow, and (d) octupolar flow.[2]Boundary conditions are shown as $+V_a$ (red), $-V_a$ (blue), and $V_a = 0$ (gray), where biased electrodes are thickened. Streamlines are shown in black, with arrows indicating flow direction.

the segments of electrode II to voltages $V_a(1, 1, 0, -1, -1, -1, 0, 1)$ [Fig. 2(a)], beginning with the segment along the positive x-axis. This results in an approximately uniform flow field $\mathbf{v} = A_1\hat{\mathbf{y}}/Br_w$ near the axis, where $A_1 = 1.18V_a$, and the next largest coefficient is $A_3 = -0.16V_a$. This flow initially advects the plasma away from the axis with no distortion; however, at later times the image charge induced in the wall leads to dynamical orbits of the plasma [18]. Alternatively, the voltage configuration $V_a(1, 0, 0, 0, 0, 0, 0, 0)$ [shown in Fig. 2(b)] generates an irrotational shear flow similar to that produced by a distant vortex structure.

A flow with a dominant $m = 2$ component can be generated by the voltage configuration $V_a(1, 0, -1, 0, -1, 0, -1, 0)$ [Fig. 2(c)], with velocity $\mathbf{v} = \epsilon(y\hat{\mathbf{x}} + x\hat{\mathbf{y}})$ where $A_2 = 0.9V_a$, the next nonzero coefficient is $A_6 = 0.3V_a$, and $\epsilon \equiv 2A_2/Br_w^2$. This is a "simple strain flow" where 2ϵ is the applied strain magnitude. This flow is frequently discussed in the fluid dynamics literature, and it has recently been studied in the 8ST [17]. Additionally, an octupolar flow (with a dominant $m = 4$ term) can be generated using the boundary conditions $V_a(1, -1, 1, -1, 1, -1, 1, -1)$ [Fig. 2(d)]. Another interesting possibility, not yet exploited, involves a simple strain flow which is rotated about the trap axis. In the rotating frame, this appears as a simple shear flow [19].

A uniform potential associated with nonzero A_0 can modify the length of the plasma, and therefore change the density (vorticity). Typically, boundary conditions are chosen such that $A_0 = 0$ to avoid this complication. The external flow can lead to a net translation of the vorticity away from the axis of the trap, for example due to an $m = 1$ component of the flow, or due to $m > 1$ flows where the plasma is not initially centered on the axis [20]. In order to avoid this complication, experiments are often restricted to short timescales where the plasma remains near the trap center.

[2] This figure is in color. See the online version for additional detail.

For the flows discussed above, the A_m are proportional to V_a, so the magnitude of the external flow velocity can be adjusted by varying V_a over time. The temporal dependence of the external strain is set using waveform generators. The only limitation is RC filtering from the electrical circuit, which presently has a ~ 1 μs time constant. Thus far, experiments with the 8ST have utilized only a square-pulse and a linear-ramp time dependence.

The influence of these external flows on an initially stable, axisymmetric vortex is an important topic in fluid dynamics, which can be studied in the 8ST. External influences can result in vortex deformation, and partial or total destruction [9, 17], with profound implications for the transport of heat, momentum, and passive scalars in a fluid. Alternatively, these external flows can be implemented serially in order to generate other non-axisymmetric initial vorticity distributions (e.g., elliptical vortices or thin filaments).

RUN PROCEDURE

The procedure for a single run cycle is shown in Fig. 3, where voltage traces applied to the 8ST electrodes are represented schematically. The run cycle typically takes 5 - 10 s. The majority of this time is occupied by the preparation of the initial vorticity profile, with the fluid experiment itself taking only < 500 μs. At the end of each run, the vorticity is diagnosed destructively using a phosphor screen diagnostic. Steps in this process are given below.

- **Programming.** First, waveform generators with 1 μs accuracy are programmed to drive the segments of electrode II with the desired voltage and time dependence.
- **Fill plasma.** Next, the trap is filled by injecting electrons. Electrode V is biased to voltage $-V_c$ and electrode I is biased to $V = -V_l$ where $|V_l| < |V_c|$. The electron source is biased to an intermediate voltage V_e, where $|V_l| < |V_e| < |V_c|$ such that electrons have sufficient energy to transit electrode I but not electrode V. Electrons become confined between electrodes I and V by scattering energy from the parallel to perpendicular direction, either through collisions or conceivably by a two-stream instability [21]. This process continues for 0.1 - 1 s, until the desired total electron number is achieved. Then, electrode I is ramped to voltage $-V_c$ to prevent further filling.
- **First diocotron damp.** The initial electron density distribution is typically offset from the symmetry axis, resulting in an $m = 1$ diocotron mode [3], where m is an azimuthal wave number. This mode is damped in 100 - 300 ms using a feedback circuit connected to two segments of electrode II.
- **Profile conditioning.** Then, the Rotating Wall (RW) is used to condition the radial density profile [3]. Here, the 4 segments of electrode VI are biased to generate a uniform electric field near the origin which rotates azimuthally at frequency f_w, injecting or removing angular momentum from the plasma. In this way, the vorticity profile $\omega(r)$ can be changed. A few examples of RW profile control and free relaxation of a profile are shown in Fig. 4.
- **Cut plasma.** The RW profile control is necessarily conducted with plasma confined between electrodes I and V, however the fluid experiments are conducted with plasma confined between electrodes I and III. Therefore, the plasma is "cut" by ramping electrode III abruptly from ground to $-V_c$. The plasma remaining between electrodes III and V is discarded.
- **Second diocotron damp.** The cutting process can result in a small amplitude $m = 1$ diocotron mode. Thus, the damping circuit is once again implemented to position the plasma centroid as close as possible to the symmetry axis.
- **Cooling.** The plasma is held for about 500 ms, and the plasma cools *via* cyclotron radiation to $T \sim 0.1$ eV with a time constant of $\tau_c = 150$ ms [22]. At this point, the plasma has the properties necessary for experiments in the fluid regime.
- **Fluid experiment.** Prior to the fluid experiment, the CCD camera is triggered with an exposure time long enough to capture the event. Then, the external flow is applied by triggering the waveform generators. The system is allowed to evolve for some time, then the segments of electrode II are grounded, and immediately thereafter electrode III is grounded such that the electrons stream along the field and impinge on the phosphor screen. The resulting light is measured with the CCD camera.
- **Dark exposure.** After diagnosis, another camera exposure is taken in the absence of plasma, and the two exposures are subtracted to eliminate background noise.

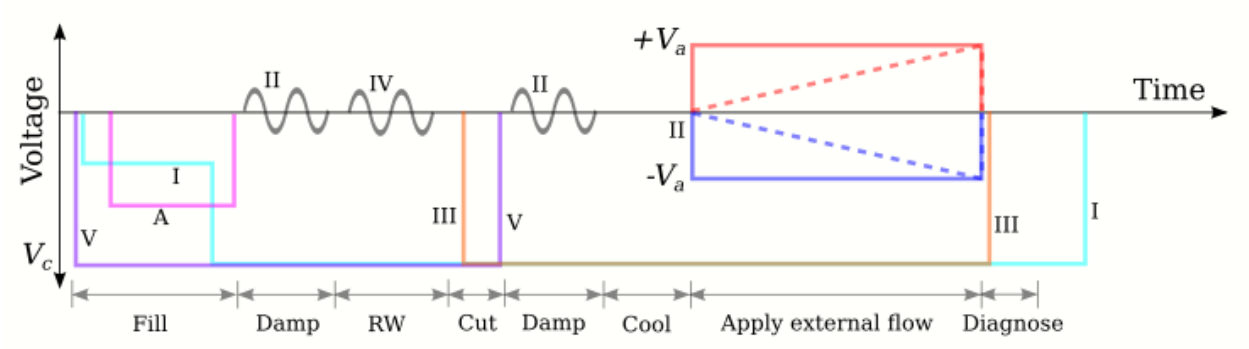

FIGURE 3. Serial steps in the experimental procedure, shown as voltage traces on the 8ST electrodes.[2] Labels A, I-V correspond to voltages on the electron source and electrodes in Fig. 1. Shown are a square pulse (solid) and linear ramp (dashed) external flow time dependence, with bipolar boundary conditions.

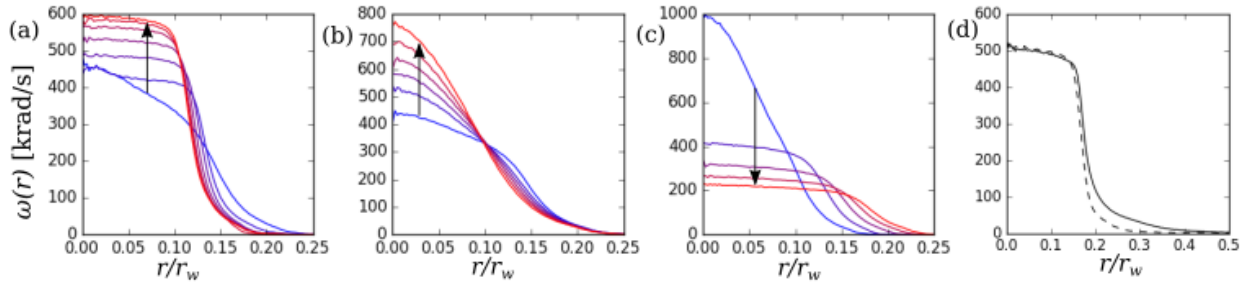

FIGURE 4. Demonstration of RW vorticity profile conditioning and profile relaxation. (a) compression to a quasi-flat profile with $f_w = 50$ kHz over 3 s (blue to red); (b) compression to a Gaussian profile with $f_w = 1$ MHz over 500 ms; (c) reverse RW expansion to a quasi-flat profile with $f_w = -1$ MHz over 1 s; (d) a profile before (solid) and after (dashed) 10 s of free relaxation, showing a small loss of particles to the wall.

The end result is a CCD image of the electron density distribution integrated over the axial direction [see, for example, Fig. 5(a)]. This data represents a measurement of the 2D vorticity field at each CCD pixel. Runs can be repeated to reduce noise, or the protocol can be varied, for example to record time series data of the vorticity evolution.

DATA ANALYSIS

Using knowledge of the applied boundary conditions, the Poisson equation $\nabla^2\psi = \omega$ is solved using a numerical finite difference algorithm to find the stream function at each CCD pixel. Then, the velocity components (v_x, v_y) are determined by numerically differentiating the stream function. Second derivatives of the stream function are then found, and used to calculate quantities such as the local strain magnitude $s(x,y) = \pm[4\psi_{xy}^2 + (\psi_{xx} - \psi_{yy})^2]^{1/2}$ (where subscripts indicate partial derivatives), and the Okubo-Weiss local stability parameter $Q(x,y) = s^2 - \omega^2$ [23]. Figure 5(a) shows a CCD image of an axisymmetric vortex on the domain axis with a quasi-flat profile and central vorticity $\omega_0 = 228$ krad/s, and Fig. 5(b) shows the same image overlaid with contours of the stream function due to an applied strain with $\epsilon^* \equiv \epsilon/\omega_0 = 0.116$. Figure 5(c) shows the stream function separatrix and velocity magnitude.

For axisymmetric vortices, it is useful to perform an azimuthal average of the vorticity data to extract the radial profile, $\omega(r) = (2\pi)^{-1} \int \omega \mathrm{d}\theta$. Examples of profiles obtained in this manner are shown in Fig. 4. Low-order spatial moments of the vorticity distribution are also calculated, including the total circulation $\Gamma = \int \omega \mathrm{d}A$, the centroid $p_i = \Gamma^{-1} \int r_i \omega \mathrm{d}A$, and the quadrupole tensor $q_{ij} = \Gamma^{-1} \int (3r_i r_j - r^2\delta_{ij})\omega \mathrm{d}A$, where r_i are the spatial coordinates and δ_{ij} is the Kronecker delta function.

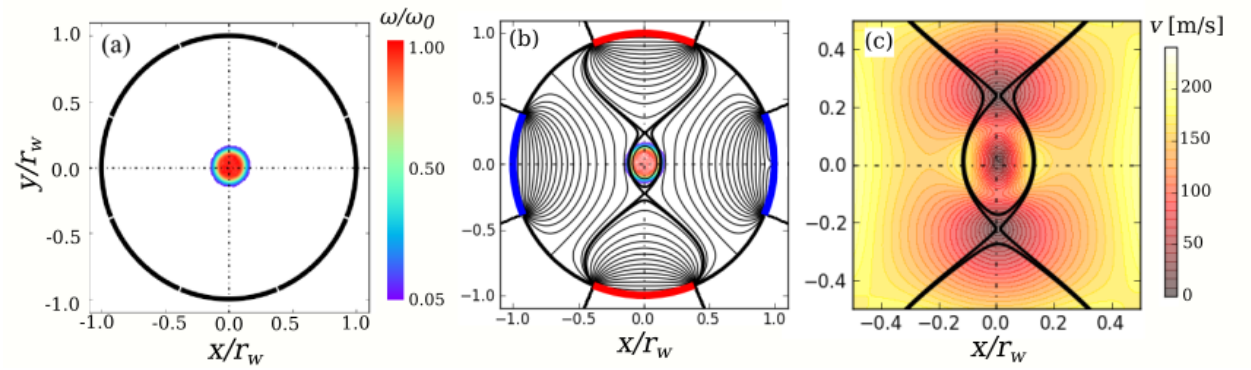

FIGURE 5. Analysis of a CCD image.[2] (a) vorticity data (color map) with $\omega_0 = 228$ krad/s, truncated at $0.05\omega_0$; (b) vorticity overlaid with numerically calculated streamlines (black lines) and separatrix (thick black line) under applied strain with $\epsilon^* = 0.116$; (c) separatrix and velocity magnitude (color map).

Elliptical modes of a vortex can be excited, for example, by an external strain flow [see Fig. 2(c)] [19], however, filamentary structures which form outside the vortex core can influence the quadrupole moment. In order to diagnose elliptical distortions of the core, a numerical routine is used to fit an ellipse to the half-maximum vorticity contour. Here, the aspect ratio λ and orientation ξ of the ellipse are fit to the set of CCD pixels with vorticity in the range $0.4 \leq \omega/\omega_0 \leq 0.6$, where ω_0 is the peak vorticity. In this way, a robust representation of elliptical distortions of the vortex core is obtained. Examples of the elliptical fitting routine are shown in Fig. 6

CALIBRATION

In order to obtain quantitative data, the CCD diagnostic spatial resolution and signal magnitude must be calibrated. From the confinement region to the phosphor screen, the electron distribution is magnified by a factor of two due to the flaring magnetic field. The flourescent light is then focused onto the CCD chip through an optical lens system. The total magnification factor can be found by preparing a plasma which fills the entire trap volume, as shown in Fig. 7(a), thus providing a measurement of r_w on the CCD image. Alternatively, the spatial calibration can be obtained using a plasma subjected to a strong external strain flow [17], as shown in Fig. 7(b). In this case, the plasma collapses to a thin filament which is advected through small gaps between the segmented electrodes. The orientation of the filament and the point at which the signal disappears give a calibration of r_w and the orientation of the segments. Figure 7(c) shows the segments of electrode II fitted using these techniques. The pixel calibration is presently 1 pixel = 33 μm.

The vorticity is calibrated by measuring the rotation rate of a slightly elliptical vortex. A quasi-flat vorticity profile is prepared, and excited to a small aspect ratio using an external strain flow, and then allowed to rotate freely at the linear rate $\mathrm{d}\xi/\mathrm{d}t = \omega_0/4$ [24]. The orientation $\xi(t)$ is measured using the fitting routine described above. Using this procedure, the measured vorticity is calibrated to the CCD signal magnitude in the vortex core. Figure 8 shows the free evolution of (λ, ξ) for three different initial values of λ. Although the aspect ratio decreases due to inviscid damping [14], the rotation rate is initially constant for $1.2 \leq \lambda \leq 1.8$, and a robust calibration of the vorticity magnitude is obtained.

The external flow field is completely specified by the electrode geometry and knowledge of the boundary conditions. However, the external flow can also be diagnosed *in situ*. For example, a uniform flow such as that shown in Fig. 2(a), when imposed suddenly, will cause the plasma to drift uniformly at velocity $v = A_1/Br_w$. This velocity can be measured using the phosphor screen, thus calibrating the external flow strength. Another calibration technique involves the simple strain flow [Fig. 2(c)]. When the normalized strain ϵ^* is sufficiently large, the plasma will behave passively, distorting elliptically with aspect ratio $\lambda(t) = \exp(2\epsilon t)$ [19]. The time dependence of the aspect ratio can be measured using the elliptical fitting routine described above, thus calibrating the external strain magnitude. Similar techniques using slowly ramped (i.e., adiabatic) uniform flows and simple strain flows also yield calibrations of the external flow.

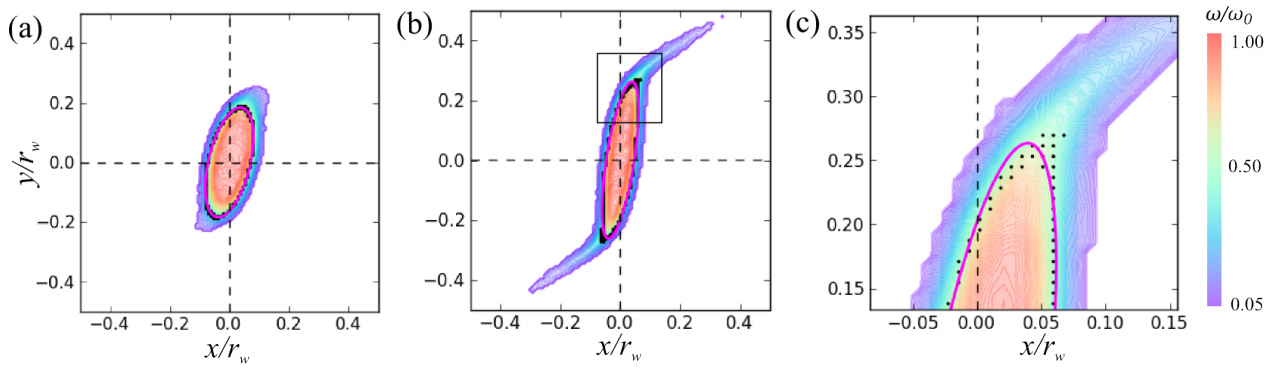

FIGURE 6. Demonstration of ellipse fitting routine, for two different instances of vorticity data (a) and (b).[2] Panel (c) shows a close-up region given by the square in panel (b). Pixels between 40-60% of ω_0 are highlighted (black dots), and the elliptical fit to these points is shown (magenta line).

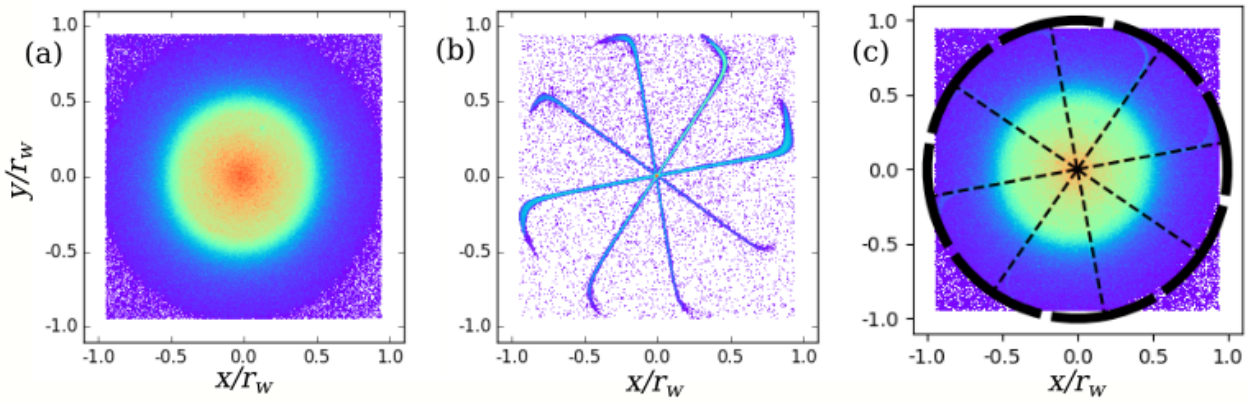

FIGURE 7. Spatial calibration of the CCD diagnostic.[2] (a) an image of plasma filling the entire trap volume; (b) overlaid images of four plasmas during destruction by an external strain flow; (c) data from panels (a) and (b) fitted with the 8-segment electrodes (black) and their orientations (dashed).

Figure 9 shows measurements of the strain magnitude. In panel (a), exponential curves are fitted to $\lambda(t)$ data to extract ϵ. In panel (b), the measured ϵ is plotted against the applied voltage V_a, showing a linear dependence for $\epsilon^* > 0.23$ with slope $\epsilon/V_a = 1923(Vs)^{-1}$ (dashed), consistent with the assumption that the plasma is behaving passively. Other techniques (uniform flow, slowly ramped flows) are consistent with this calibration factor, leading us to conclude that the strain calibration technique described here is robust. However, the calibration factor disagrees slightly from the value calculated from the voltage and electrode geometry, $\epsilon/V_a = 2212(Vs)^{-1}$ (solid). Presently, the exact source of this discrepancy is not understood.

LIMITATIONS TO THE PLASMA/FLUID ANALOGY

In order for the plasma/fluid analogy to be valid, the perpendicular dynamics of the plasma must follow the Drift-Poisson equations (Eq. 1). This amounts to a separation of spatial and temporal scales. Frequency scales must obey $f_g \gg f_b \gg f_v \gg f_c$ where $f_g = eB/m$ is the gyrofrequency; $f_b = \sqrt{T/m}/L_p$ is the axial bounce frequency with L_p the axial length of the plasma and $\sqrt{T/m}$ the thermal velocity; f_v is the frequency scale of the fluid motion; and f_c the electron-electron collision frequency. Spatial scales must obey the relations $r_g \ll r_v, r_w \ll L_p$, where r_g is the gyroradius and r_v the scale of vorticity features. Described here are non-ideal, non-2D, and non-fluid effects which arise when these conditions are not satisfied. Also given are the degrees to which these assumptions are satisfied in the 8ST.

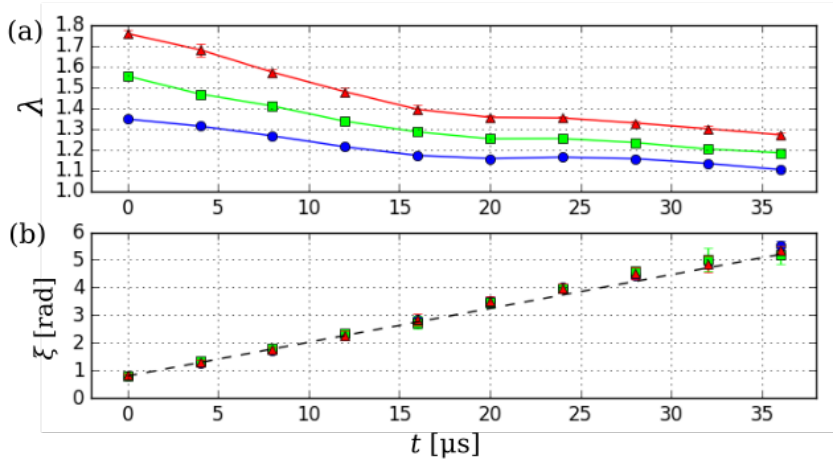

FIGURE 8. Vorticity calibration process. (a) $\lambda(t)$ and (b) $\xi(t)$ are shown for a freely rotating quasi-flat vortex excited to $\lambda = 1.35$ (circles), 1.55 (squares), and 1.75 (triangles). Included is a linear fit (dashed) to the $\xi(t)$ data for $0 \leq t \leq 16$ μs, where $\omega_0 = 488$ krad/s.

- **3D effects.** The confinement electrodes (I, III, and V) produce a radial vacuum electric field which gives rise to an $\mathbf{E}\times\mathbf{B}$ background rotation known as the "magnetron" drift [3]. This effect is minimized by using a large aspect ratio trap, with $r_w \ll L_p$. In the 8ST, $r_w/L_p = 10$ and the magnetron rotation frequency near the origin is ~ 150 Hz, three orders of magnitude below f_v. Additionally, 3D geometric effects can be introduced by a misalignment of the electrode axis with the magnetic field. However, to our knowledge no significant 3D effects are observed in the 8ST.
- **Small spatial scales.** At small spatial scales, the fluid analogy can be broken by finite gyroradius effects and discrete particle effects. In the 8ST the gyroradius is $r_g = 0.5$ μm, 2 orders of magnitude below the CCD resolution. Discrete particle effects are expected at spatial scales approaching the inter-particle spacing, which is $(nL_p)^{-1/2} = (\omega B \epsilon_0 L_p/e)^{-1/2} = 0.125\ \omega^{-1/2}$ mm. Therefore, the inter-particle spacing approaches the CCD pixel size for $\omega \approx 14$ rad/s, 4 orders of magnitude lower than the typical central vorticity. Such a signal would be well below the CCD noise floor, which is typically ~ 10 krad/s.
- **Viscosity.** Viscosity is present in a pure electron plasma as a result of electron-electron collisions; however it differs fundamentally from the hydrodynamic viscosity appearing in the Navier-Stokes equations. In general, the viscosity varies with electron density inside the plasma. There is no viscosity outside of the plasma (i.e., in irrotational regions of the flow), and so the system obeys free-slip boundary conditions. For a more detailed discussion of electron plasma viscosity, see Ref. [25].
- **Plasma expansion.** For a plasma isolated from the boundary, viscosity itself cannot drive net radial vorticity transport, in contrast with viscous hydrodynamic vortices [26]. In practice, small asymmetries and construction errors in the apparatus (for example, gaps between the segmented electrodes) can drive outward radial transport of the plasma [27], thus behaving like an effective viscosity. In the 8ST, the ratio of the decay time of the central vorticity to the vortex rotation period is $> 10^6$ [see Fig. 4(d)].
- **Plasma re-entry.** For sufficiently large values of strain magnitude, some or all of the electron distribution may be advected out of the trap through the small gaps between the 8-segment electrodes [17]. It is routinely observed that some electrons *orbit the biased segment and return into the trap* (c.f. Fig. 10). Apparently, these particles are confined axially and obey $\mathbf{E}\times\mathbf{B}$ drift dynamics in the vacuum region outside the segmented electrodes. Although interesting, this behavior can be detrimental to the experiments, since the re-entrant circulation can modify the dynamics of the remaining circulation.
- **Dump rotation.** During the imaging process, the electrons must travel axially from the 8-segment region to the phosphor screen. In this time, the density distribution continues to drift in the plane perpendicular to $\mathbf{B}$. For example, an elliptical vortex may rotate as much as 10° during diagnosis [17]. The amount of rotation is measured, and the data corrected accordingly.

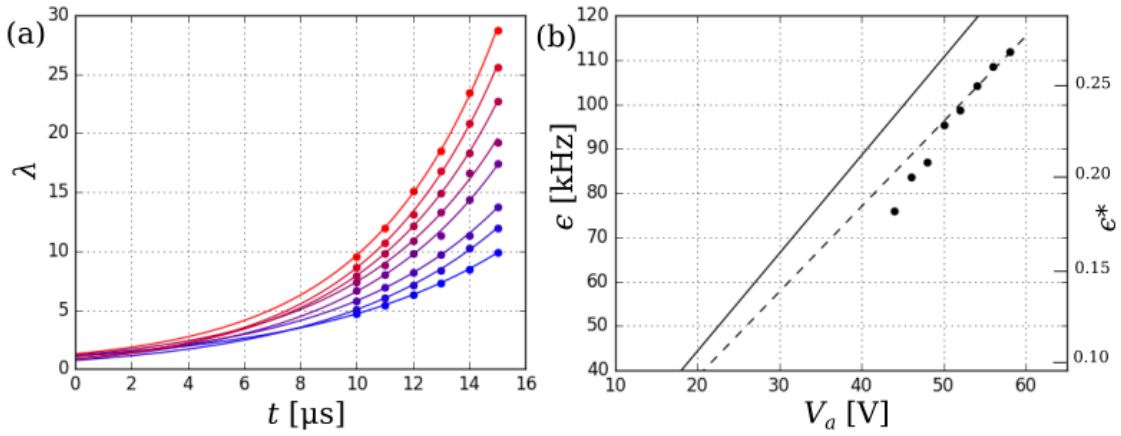

FIGURE 9. Strain calibration process. (a) measurements of $\lambda(t)$ for $\epsilon^* = 0.18 - 0.27$ (blue to red), with $\omega_0 = 420$ krad/s; (b) measurements of $\epsilon(V_a)$ given by exponential fits to $\lambda(t)$. The calibrated strain to voltage ratio (dashed) is compared to the calculated value (solid).

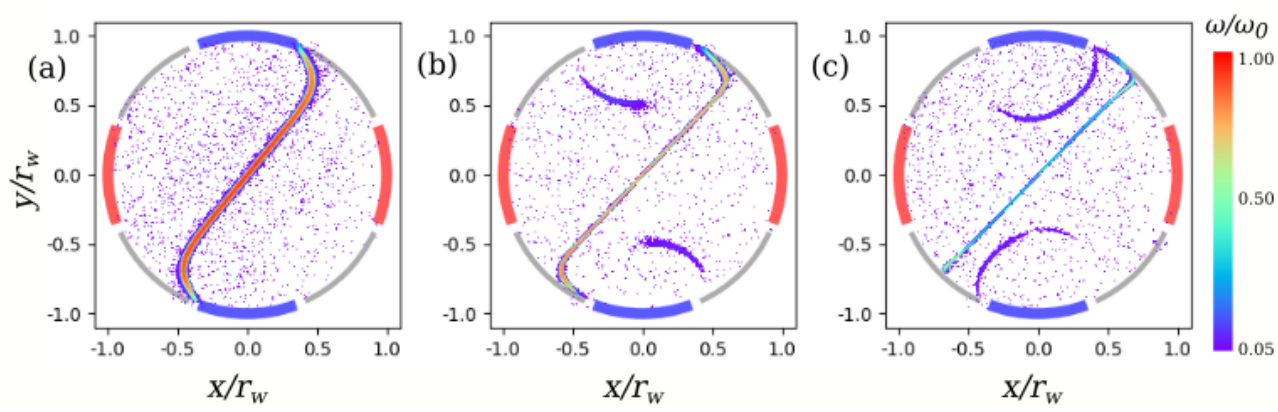

FIGURE 10. Demonstration of electron re-entry after a straining event with $\epsilon^* = 0.25$, at times $t =$ (a) 20, (b) 30, and (c) 40 μs.[2] Electrons are advected through gaps between segmented electrodes, then drift around the biased segment and eventually return to the trap volume.

The effects described in this section break the 2D fluid analogy, and so care must be taken to avoid them. In most cases, this can be accomplished by choosing appropriate values of the vorticity and experiment duration, such that the necessary separation of scales is acheived.

SUMMARY

The 8ST apparatus discussed here is a Penning-Malmberg electron plasma confinement device designed specifically to study the physics of ideal 2D fluids subject to external flows. This is accomplished using a segmented electrode which extends over the entire length of the plasma. The individual segments can be biased to create a 2D electric potential which gives rise to an externally imposed, irrotational $\mathbf{E} \times \mathbf{B}$ flow. Specific details of the 8ST have been described, including its capabilities, limitations, and the standard operating procedure.

The experimental conditions described here are difficult to achieve with water tanks or other types of electron plasma devices. The rotating wall technique [3] allows for excellent control over the initial (axisymmetric) vorticity profile. In particular, quasi-flat profiles are readily obtained in the 8ST (c.f. Fig. 4),

whereas in a traditional laboratory fluid (i.e., water) vorticity gradients are quickly reduced due to viscosity [9]. These flat profiles can be used to test the predictions of well-known theoretical work assuming a piecewise-constant elliptical vorticity distribution [6, 19]. Additionally, the 8ST allows for arbitrary strength and time dependence of the external flow, since the boundary conditions are specified in pure 2D. Recent work in the 8ST has studied dynamical orbits and destruction of quasi-flat vortices in external 2D strain flows [17]. Current experiments are using the rotating wall profile control technique to study departures from the elliptical patch theory when the profile smoothness is varied, in an attempt to model realistic vortices [28].

Future experiments with the 8ST or similar devices could investigate other types of external flows (shear, octupole, etc.) as well as time-dependent flows. For example, a Gaussian shear or strain pulse could be used to mimic a vortex scattering event; a strong transient strain pulse could be used to generate a filament of vorticity and study its dynamics; a strain flow which is sinusoidal in time could be implemented to study resonant behavior and the onset of turbulence; and relaxing turbulence could be studied in the presence of a background strain flow.

ACKNOWLEDGMENTS

We wish to thank D. H .E. Dubin for helpful conversations. This work is supported by plasma partnership grant DOE No. DE-SC0016532.

REFERENCES

[1] C. F. Driscoll and K. S. Fine, *Phys. Fluids B* **2**, 6 (1990).
[2] D. G. Dritschel and B. Legras, *Phys. Today* **46**, 44-51 (1993).
[3] J. R. Danielson, D. H. E. Dubin, R. G. Greaves, C. M. Surko, *Rev. Mod. Phys.* **87** 247-306 (2015).
[4] P. W. Terry, *Rev. Mod. Phys.* **72** 109-165 (2000).
[5] P. Godon and M. Livio, *Astrophys. Journal* **523** 350-356 (1999).
[6] D. W. Moore and P. G. Saffman, "Structure of a line vortex in an imposed strain," in *Aircraft wake turbulence and its detection,* edited by J. H. Olsen, A. Golburg, and M. Rogers (Plenum Press, New York, 1971) pp. 339-354.
[7] G. A. Voth, G. Haller, J. P. Gollub, *Phys. Rev. Lett.* **88** 254501 (2002).
[8] P. Tabeling, *Phys. Reports* **362** 1-62 (2002).
[9] R. R. Trieling, M. Beckers, G. J. F. Van Heijst, *J. Fluid Mech.* **345** 165-201 (1997).
[10] K. S. Fine, A. C. Cass, W. G. Flynn, C. F. Driscoll, *Phys. Rev. Lett.* **75** 3277-3280 (1995).
[11] D. Durkin and J. Fajans, *Phys. Fluids* **12** 289-293 (2000).
[12] T. B. Mitchell and C. F. Driscoll, *Phys. Fluids* **8** 1828-1841 (1996).
[13] Y. Kawai, Y. Kiwamoto, Y. Soga, J. Aoki, *Phys. Rev. E* **75** 066404 (2007).
[14] D. A. Schecter, D. H. E. Dubin, A. C. Cass, C. F. Driscoll, I. M. Lansky, T. M. O'Neil, *Phys. Fluids* **12** 2397-2412 (2000).
[15] R. Chu, J. S. Wurtele, J. Notte, A. J. Peurrung, and J. Fajans, *Phys. Fluids B*, **5** 7 2378-2386 (1993).
[16] D. L. Eggleston, *Phys. Plasmas* **1**, 3850-3856 (1994).
[17] N. C. Hurst, J. R. Danielson, D. H. E. Dubin, C. M. Surko, *Phys. Rev. Lett.* **117** 235001 (2016).
[18] N. C. Hurst, J. R. Danielson, C. J. Baker, C. M. Surko, *Phys. Rev. Lett.* **113** 025004 (2014).
[19] S. Kida, *J. Phys. Soc. Japan* **50** 3517-3520 (1981).
[20] J. Fajans, E. Yu. Backhaus, E. Gilson, *Phys. Plasmas* **7** 3929-3933 (2000).
[21] T. Mohamed, H. Imao, N. Oshima, A. Mohri, Y. Yamazaki, *Phys. Plasmas* **18** 032507 (2011).
[22] T. M. O'Neil, *Phys. Fluids* **23** 725-731 (1980).
[23] J. Weiss, *Physica D* **48** 273-294 (1991).
[24] P. G. Saffman, *Vortex Dynamics* (Cambridge University Press, 1992) pp. 167.
[25] J. M. Kriesel and C. F. Driscoll, *Phys. Rev. Lett.* **87** 135003 (2001).
[26] T. M. O'Neil, *Phys. Fluids* **23** 2216-2218 (1980).
[27] J. M. Kriesel and C. F. Driscoll, *Phys. Rev. Lett.* **85** 2510-2513 (2000).
[28] N. C. Hurst, manuscript in preparation.